

Revealing the Degradation and Self-Healing Mechanisms in Perovskite Solar Cells by Sub-Bandgap External Quantum Efficiency Spectroscopy

Yuanhang Cheng,* Xixia Liu, Zhiqiang Guan, Menglin Li, Zixin Zeng, Ho-Wa Li, Sai-Wing Tsang,* Armin Gerhard Aberle, and Fen Lin*

Ion dissociation has been identified to determine the intrinsic stability of perovskite solar cells (PVSCs), but the underlying degradation mechanism is still elusive. Herein, by combining highly sensitive sub-bandgap external quantum efficiency (s-EQE) spectroscopy, impedance analysis, and theoretical calculations, the evolution of defect states in PVSCs during the degradation can be monitored. It is found that the degradation of PVSCs can be divided into three steps: 1) dissociation of ions from perovskite lattices, 2) migration of dissociated ions, and 3) consumption of I^- by reacting with metal electrode. Importantly, step (3) is found to be crucial as it will accelerate the first two steps and lead to continuous degradation. By replacing the metal with more chemically robust indium tin oxide (ITO), it is found that the dissociated ions under light soaking will only saturate at the perovskite/ITO interface. Importantly, the dissociated ions will subsequently restore to the corresponding vacancies under dark condition to heal the perovskite and photovoltaic performance. Such shuttling of mobile ions without consumption in the ITO-contact PVSCs results in harvesting–rest–recovery cycles in natural day/night operation. It is envisioned that the mechanism of the intrinsic perovskite material degradation reported here will lead to clearer research directions toward highly stable PVSCs.

perovskites have attracted tremendous research interest in the photovoltaic community worldwide.^[1] Although the world record power conversion efficiency (PCE) of perovskite solar cells (PVSCs) has been increased to 25.2%, comparable to that in crystalline silicon solar cells, the long-term stability issue remains a major challenge for PVSCs in order to compete with the silicon technology.^[2] It has already been demonstrated that the degradation of metallic halide perovskites can be prevented from reacting with external stimuli of moisture and oxygen by advanced encapsulation techniques.^[3] However, the degradation by reacting with interlayers and ion dissociation in perovskite itself still remains a complex issue to be resolved.

Recently, the failure of organic charge-transporting interlayers and the diffusion of metal contacts have been recognized as the key factors responsible for the instability of PVSCs. Various strategies have been employed to overcome such device-structure- and material-related degradation. For example, Yang and co-workers

Owing to the appealing optoelectronic properties, such as large absorption coefficient, long charge carrier diffusion length, and carrier lifetime, the organic–inorganic metallic halide

have demonstrated a significant enhancement in PVSC stability with an all-metal-oxide device structure to avoid using organic charge-transporting layers.^[4] Grätzel and co-workers have shown that PVSCs using inorganic CuSCN/reduced graphene oxide bilayer as the top hole-transporting layer retained over 95% of their initial efficiency after aging for 1000 h operating at the maximum power point (MPP). Such an improvement is ascribed to the robust property of the inorganic charge-transporting materials as compared to its organic counterpart 2,2',7,7'-tetrakis[*N,N*-di(4-methoxyphenyl)amino]-9,9'-spirobifluorene.^[5] In addition, metal-contact-induced perovskite degradation has also been reported and is getting more attention in the PVSC community. Han and co-workers demonstrated that by inserting an iodide diffusion barrier between perovskite and Ag can successfully suppress the diffusion of I^- ions by 10^3 – 10^7 times and thus improve the device stability.^[6] Meanwhile, McGehee and co-workers have shown that Ag can diffuse across even a thick (over 100 nm) sputtered indium–tin oxide (ITO) layer and react with the perovskite film, inducing device degradation.^[7] Although PVSCs using other metals such as Cu and Au as the electrodes have been proven to be relatively

Dr. Y. Cheng, Dr. H.-W. Li, Prof. A. G. Aberle, Dr. F. Lin
Solar Energy Research Institute of Singapore
National University of Singapore
Singapore 117574, Singapore
E-mail: serchy@nus.edu.sg; lin.fen@nus.edu.sg

Dr. X. Liu
Department of Materials Science and Engineering
College of Engineering
Peking University
Beijing 100871, China

Dr. Z. Guan, Dr. M. Li, Z. Zeng, Prof. S.-W. Tsang
Department of Materials Science and Engineering
Center of Super-Diamond and Advanced Films (COSDAF)
City University of Hong Kong
Hong Kong SAR 999077, China
E-mail: saitsang@cityu.edu.hk

 The ORCID identification number(s) for the author(s) of this article can be found under <https://doi.org/10.1002/adma.202006170>.

DOI: 10.1002/adma.202006170

more stable than Ag, almost all metal electrodes tend to react with the halogens in perovskites and cause damage.^[8]

Another fundamental factor that determines the stability of the metal halide perovskites is the dissociation and migration of ions from the perovskite crystal lattices. Several theoretical studies have suggested that the formation of ionic defects such as vacancies, interstitials, and antisites accompanied by ion migration would result in irreversible decomposition of the perovskite lattice structure.^[9] It has also been demonstrated that both weakly coordinated perovskite anions and cations can be dissociated under stress of light, heat, and electrical field.^[10] In particular, as the halide vacancies have the lowest formation energy,^[11] halogen ions such as iodine ions (I⁻) are highly mobile with diffusion coefficients as high as 10⁻¹² cm² s⁻¹.^[6] Consequently, the continuous migration of the dissociated ions can result in chemical decomposition of the perovskites. Therefore, compositional engineering and defect passivation have been developed to chemically localize the mobile ions and passivate the structural defects in perovskite crystals.^[10a,12] Undoubtedly, understanding the degradation mechanism of PVSCs is of the utmost importance for the technology, and a direct experimental approach which can monitor the ion dissociation during device operation would shed light on this important issue.

In this work, we employed a new approach using highly sensitive sub-bandgap external quantum efficiency (s-EQE) spectroscopy to monitor the ion dissociation process in methylammonium lead iodide (MAPbI₃)-based PVSCs during the degradation. We first compared the stability of PVSCs with Ag and ITO as the electrode at the MPP. The s-EQE was then performed to measure the sub-bandgap spectra of the devices at different time intervals during the degradation. The change of the spectral characteristics was further analyzed by Gaussian fitting and compared with the defect states energy obtained by theoretical calculation. Cycling test and several other spectroscopy measurements were also performed to investigate the degradation and self-healing processes in the perovskites. Finally, based on the above experimental findings, the degradation mechanism and strategy to further improve the PVSCs stability will be discussed.

In order to investigate the ion-dissociation-induced degradation in PVSCs, it is important to deconvolve other factors. The PVSC degradation induced by reaction between perovskite and Ag has been well studied previously.^[13] Similar degradation phenomena of the Ag-contact devices using either organic or inorganic interlayers were also observed as depicted in Figures S1–S3 (Supporting Information). We sought to investigate the Ag diffusion into the MAPbI₃ perovskite layer by energy-dispersive X-ray (EDX) spectroscopy. As shown in Figure 1a, the Ag electrode was removed by a lift-off process, and the [6,6]-phenyl-C61-butyric acid methyl ester (PC₆₁BM)/aluminum-doped zinc oxide (AZO) layers were then washed away with chlorobenzene. As shown in Figure 1b, there is a large amount of Ag particles detected on the perovskite surface for the device after the MPP tracking test for 10 h, whereas there is a negligible amount of Ag particles detected in the fresh device. Therefore, the PC₆₁BM/AZO bilayer cannot completely prevent Ag from diffusion to the perovskite, which severely hinders the investigation of the intrinsic degradation of the perovskite materials during the device operation.

To overcome the above-mentioned issue, we attempted to eliminate the metal-contact diffusion-induced degradation by replacing Ag with ITO as the top electrode. Figure 1c,d shows the device structure and the corresponding *J*–*V* characteristics. Although the ITO-contact MAPbI₃ PVSC has a lower PCE of 15.5% due to the increased contact resistance and reduced optical absorption, its MPP stability is significantly higher. The device dropped to 80% of its initial PCE after operating for 200 h (*T*₈₀ = 200 h), and it remained to have the similar efficiency even after 1000 h, as shown in Figure 1e. On the other hand, the Ag device with 2,9-dimethyl-4,7-diphenyl-1,10-phenanthroline (BCP) became electrically shorted after 10 h of operation, while the Ag device with AZO reached the *T*₈₀ after 30 h. It is clear that the continuous degradation observed in the Ag-contact devices is due to the diffusion of Ag atoms into the perovskite layer. It also hints that the initial 20% PCE drop in the ITO-contact device could be primarily associated with the intrinsic degradation of the perovskite layer itself.

Considering the nature of the material properties in perovskite, the reduced photovoltaic performance should be caused by the increasing amount of defect states created by ion dissociation and migration. Photothermal deflection spectroscopy (PDS) and thermal admittance spectroscopy (TAS) have been demonstrated to be capable of measuring defect states density and energy in perovskites, respectively.^[14] However, PDS can only measure the standalone perovskite film and TAS relies on model fitting. Ultimately, understanding the degradation mechanism requires a direct probing method, which can monitor the defect states during the device degradation. Here, we employed a highly sensitive s-EQE spectroscopy to probe the photocurrent contributed by the sub-bandgap absorption. Our s-EQE system has been optimized with a sensitivity of up to 10⁻⁷%, which is able to probe sub-picoampere photocurrent generated in the photoexcited defect states. Figure 2a shows the EQE spectra in the range of 0.8–2.0 eV for both Ag and ITO-contact devices in log scale. The above gap EQE spectra are depicted in Figure S4 (Supporting Information). Before light soaking, both devices have similar s-EQE spectral characteristics with a gradual decrease from 10⁻⁵% to 10⁻⁶% toward lower energy in the below gap region. Interestingly, upon light soaking, the s-EQE of the Ag-contact PVSC shows an increase in the entire sub-bandgap range from 0.8 to 1.4 eV, while the ITO-contact device has only an increase at around 1.4 eV. Since the s-EQE signal depends on both the amount and energy of the states being excited, the results bring insight into the different nature of defect states generated in Ag-contact and ITO-contact PVSCs during the device operation.^[15]

We further analyzed the evolution of the s-EQE spectra in the sub-gap region by calculating the difference after and before light soaking, i.e., Δ*s*-EQE = *s*-EQE_{soaked} – *s*-EQE_{fresh}. The corresponding Δ*s*-EQE spectra were fitted by a Gaussian model, which has been widely used to describe the density of defect states in perovskites^[16]

$$f = \frac{A}{\sqrt{2\pi}\sigma} \exp\left(-\frac{(x-\mu)^2}{2\sigma^2}\right) \quad (1)$$

where μ is the peak energy, σ is the standard deviation, and A is the proportional constant. We first analyzed the ITO-contact PVSC as it had no metal diffusion issue. Figure 2b shows its

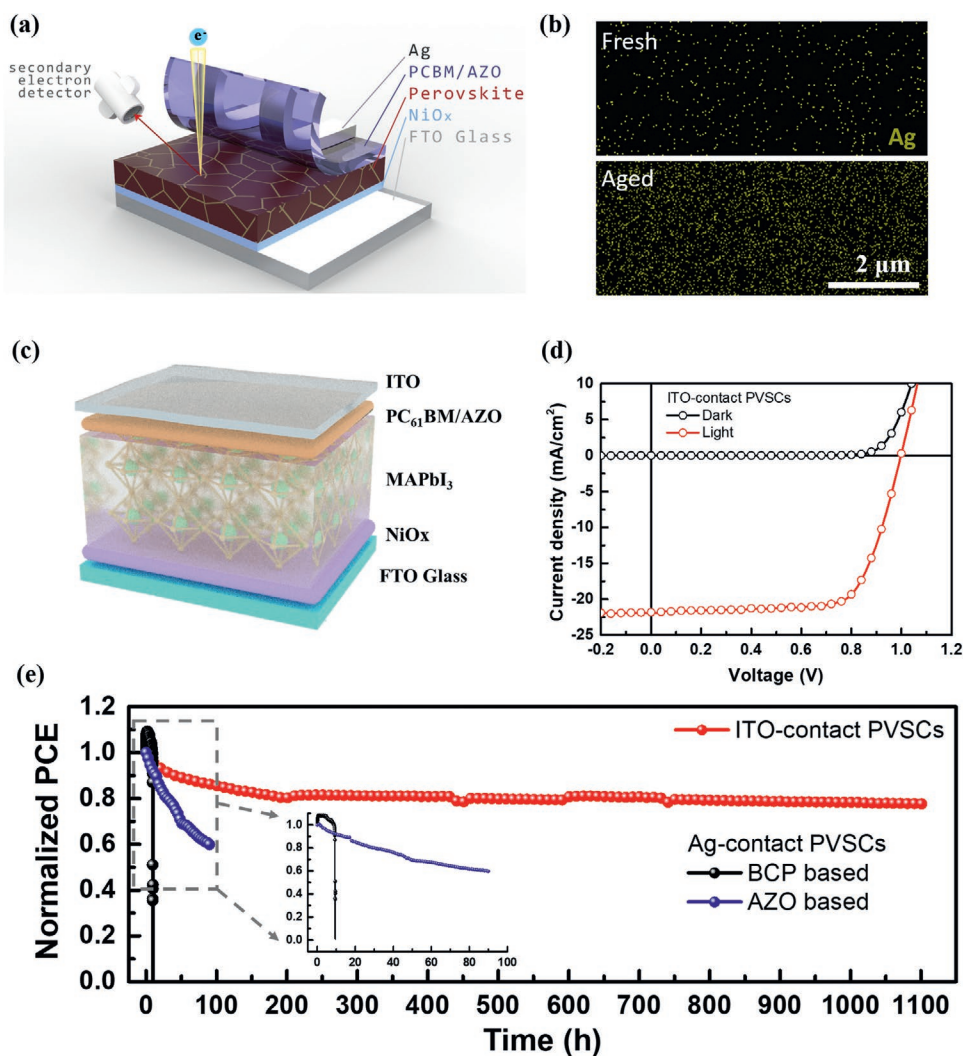


Figure 1. a) Illustration of EDX mapping to detect Ag diffusion through PC₆₁BM/AZO bilayer. The Ag electrode was peeled off by an adhesive tape and the PC₆₁BM/AZO bilayer was removed by washing the film with chlorobenzene. b) EDX mapping of Ag element at the perovskite surface for an AZO-based Ag-contact PVSC before and after MPP tracking under light soaking. c) Device structure illustration of ITO-contact PVSCs. d) *J*-*V* characteristics of the ITO-contact PVSCs. e) MPP tracking of ITO-contact PVSCs and Ag-contact PVSCs based on BCP and AZO buffer layers.

Δ s-EQE spectra and Gaussian fitting results, where only two defect states have been observed with average transition energies of 1.40 eV (defect I) and 1.22 eV (defect II). Then we assumed that the two defects in the Ag-contact device should have similar transition energy and standard deviation. As a result, four peaks were extracted in the Ag-contact PVSC at 1.40 eV (defect I), 1.22 eV (defect II), 1.08 eV (defect III), and 0.95 eV (defect IV). The fitting parameters for the 10 h light-soaked devices are listed in Table 1, and the complete fitting results are depicted in Table S1 (Supporting Information).

Recently, theoretical analysis has been done on finding the energetics of point defects in perovskites. It is found that vacancies and interstitials with smaller formation energy tend to form shallow defects, while the antisites with larger formation energy are prone to form deeper defects.^[9,11,17] To identify the defect states, we extracted the energy level of various defect states allocated in the perovskite bandgap from previous reports, as reviewed by Steele and co-workers as shown in Figure S5

(Supporting Information), and summarized the possible defects corresponding to the peak energies extracted from the s-EQE results in Table S2 (Supporting Information). According to the calculated defect energy level, we can ascribe the defect state I (1.40 eV) to the vacancy and interstitial of V_{Pb}, V_I, I_i, and MA_i, as those have lower formation energy. Defect II at 1.22 eV can be assigned to the interstitial defects of I_i and Pb_i. Defect III at 1.08 eV can be assigned to the vacancy and antisite of V_{Pb} and I_{Pb}. And defect IV at 0.95 eV can be assigned to the interstitial and antisite of I_i and I_{MA}. It should be noted that the Ag atoms/ions' diffusion into perovskite lattice is possible to create defects and contribute to the s-EQE signal. However, such an Ag-related defect energy level calculation is not available in existing literature reports. Further investigation is needed to verify the proposed mechanism.

To understand the degradation mechanism, we sought to associate the above-observed defect states with the change of chemistry in perovskites. Based on the above defect

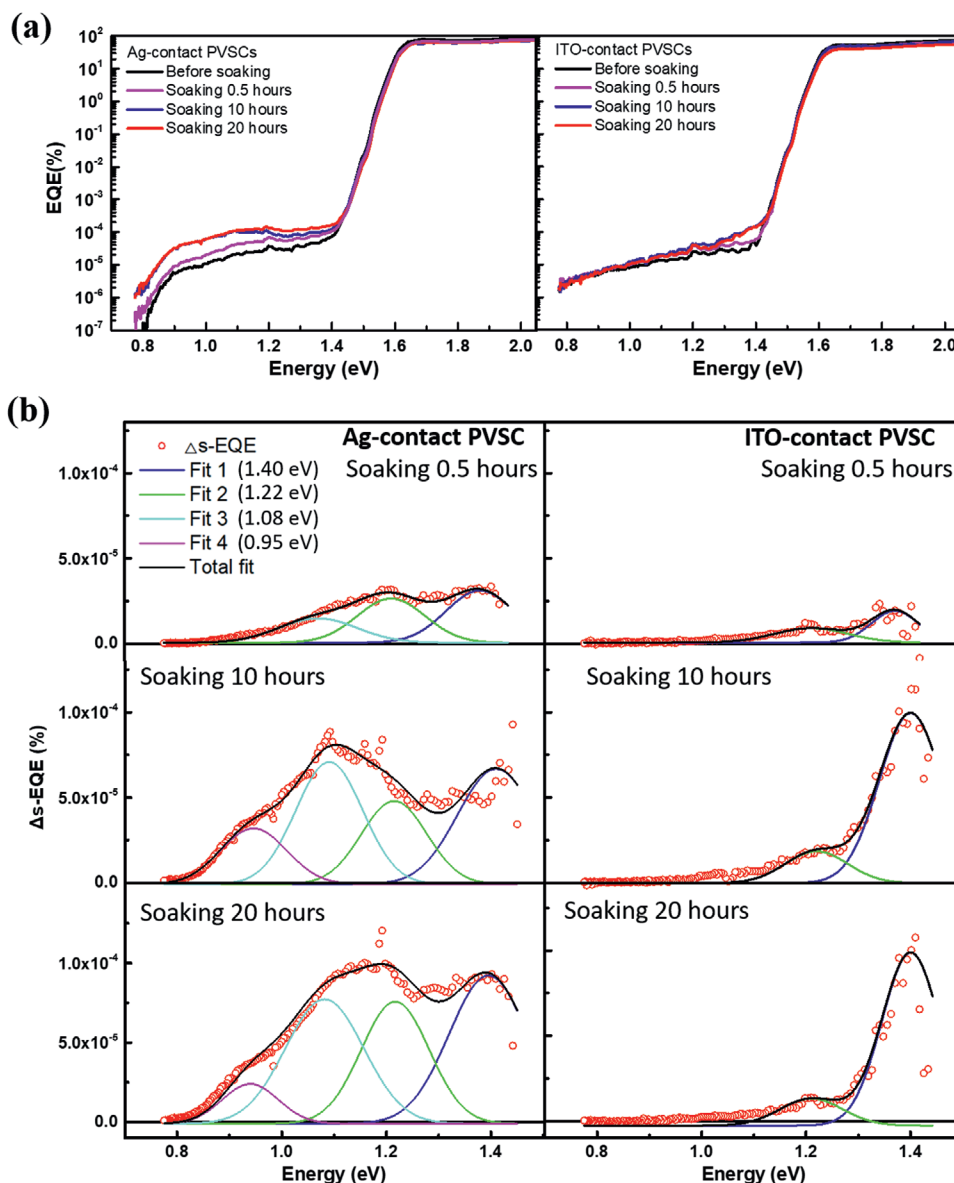


Figure 2. a) EQE spectra of Ag-contact and ITO-contact PVSCs upon light soaking for different durations. b) Δs -EQE spectra (open circle) and Gaussian fitting results (lines) of Ag-contact and ITO-contact PVSCs upon light soaking for 0.5, 10, and 20 h, respectively.

identification and the Δs -EQE results, we can illustrate the degradation mechanism for the ITO-contact and Ag-contact PVSCs as follows.

Table 1. Parameters used in Δs -EQE fitting with Gaussian functions for Ag-contact and ITO-contact PVSCs after light soaking at MPP for 10 h.

	μ [eV]	σ	A	μ [eV]	σ	A
	Ag-contact PVSCs			ITO-contact PVSCs		
Defect state I	1.41	0.073	1.2×10^{-5}	1.40	0.060	1.5×10^{-5}
Defect state II	1.22	0.063	7.7×10^{-6}	1.22	0.060	2.8×10^{-6}
Defect state III	1.08	0.064	1.2×10^{-5}	–	–	–
Defect state IV	0.95	0.063	5.2×10^{-6}	–	–	–

- i) For the ITO-contact PVSCs, upon light soaking, ion dissociation in perovskite lattice would initiate the formation of vacancy defects with lower formation energy, such as V_{Pb} , V_I , and V_{MA} . Then the migration of these dissociated ions along the perovskite lattice would create interstitial defects such as I_i , MA_i and Pb_i . Considering the defect energy level as discussed above, the V_{Pb} , V_I , I_i , and MA_i defects contribute to the Δs -EQE peak at 1.40 eV, while defects I_i and Pb_i contribute to the peak at 1.22 eV. Since the dissociated ions would accumulate at the perovskite/ITO interface and establish an internal electrical field, which suppress further ion dissociation and migration from the perovskite lattice, the Δs -EQE signal has negligible change at longer soaking time from 10 to 20 h.
- ii) For the Ag-contact PVSCs, upon light soaking, the initial ion dissociation and migration processes would be similar to the

ITO-contact PVSCs with the formation of those vacancies and interstitials, contributing the Δs -EQE peaks at 1.40 and 1.22 eV. The different defect formation process in Ag-based device is the possible reaction between the dissociated I^- ions and the diffused Ag particles, which trigger further ion dissociation and migration from the perovskite lattice in the bulk. Therefore, the peak intensities of Δs -EQE at 1.40 and 1.22 eV have been increased while increasing the light soaking time. In addition, the continuous ion dissociation with increased ion concentration would also increase the probability of forming antisite defects, for example, the I^- ion fills the Pb and MA vacancies to form I_{Pb} and I_{MA} . These two defects contribute to the Δs -EQE peaks at 1.08 and 0.95 eV, respectively.

The above results and analyses suggest that the number of dissociated ions in ITO-contact device would be saturated after 10 h of light soaking, and these ions would not further react with other coordinated ions in the perovskite lattice. It paves a way that the dissociated ions could restore the vacancies and recover the photovoltaic performance. On the other hand, the formation and increasing amount of antisite defects

in the Ag-contact device would result in permanent damage to the perovskite lattice. We intended to “rest” the PVSCs by putting the devices in dark after light soaking to investigate the recovery effect of defect states. **Figure 3a** show the s-EQE spectra of the Ag-contact and ITO-contact PVSCs before and after light soaking for 10 h, followed by resting in dark overnight. Notably, the s-EQE signal of the ITO-contact PVSC at 1.4 eV has reduced after resting in dark, suggesting that a self-healing process occurs during the resting period. On the contrary, the Ag-contact device does not exhibit such self-healing behavior, and the s-EQE signal remains the same even after the light soaking. We further fitted the Δs -EQE spectra of both PVSCs after resting with the Gaussian model as shown in **Figure 3b**. Compared to the Δs -EQE spectra after light soaking, the intensities of the two peaks at 1.40 and 1.22 eV of the ITO-contacted PVSC are significantly reduced, indicating that the vacancies and interstitials have been restored. However, such a recovery of the perovskites lattice is incomplete because these two peaks still can be observed with weak intensities. For the Ag-contacted PVSC, although the reduced peak intensities with slight defects’ recovery have been observed as well after resting

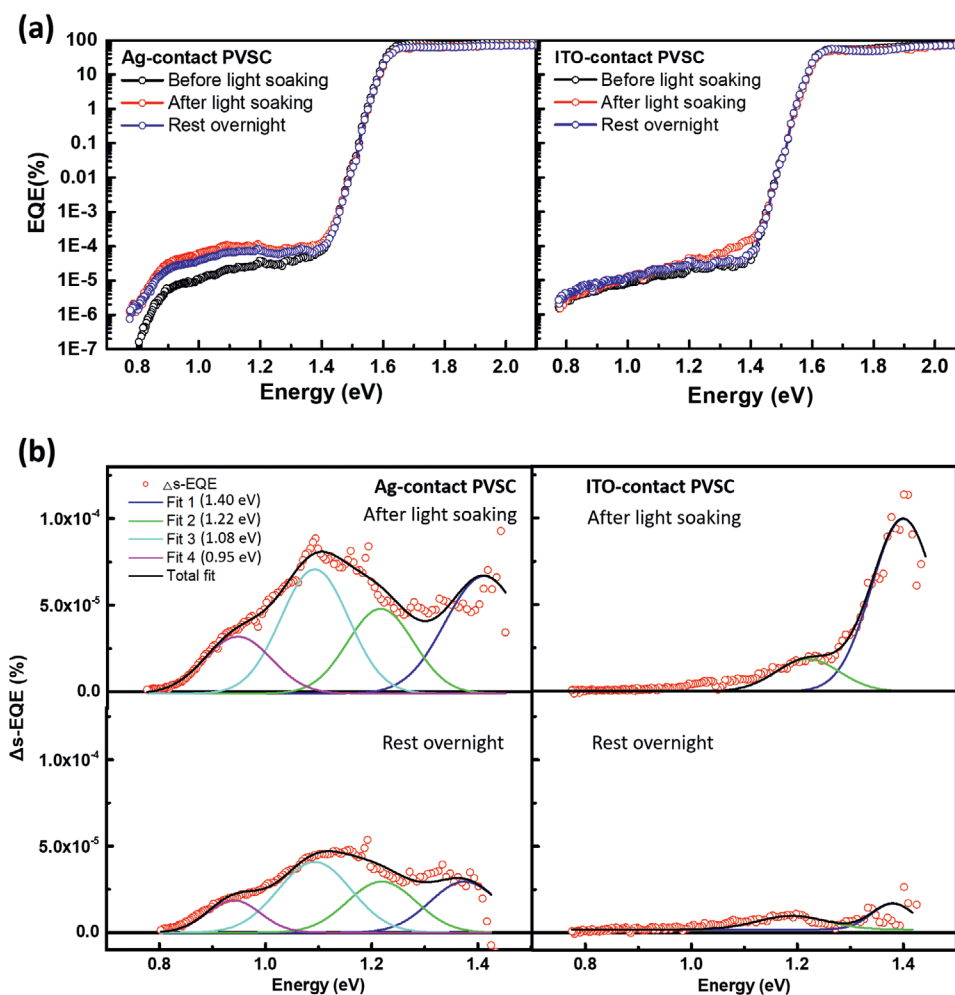


Figure 3. a) EQE spectra of Ag-contact and ITO-contact PVSCs before and after light soaking for 10 h, as well as after resting in the dark overnight. b) Δs -EQE spectra (open circle) and Gaussian fitting results (lines) of Ag-contact and ITO-contact PVSCs after light soaking (10 h) and resting overnight.

overnight, the continuous degradation of the Ag-contact PVSC is believed to be the corrosion of charge-transporting layer and Ag electrode. According to the above results, we speculated that in the Ag-contact PVSCs, the dissociated ions, especially I^- ions driven by the internal electrical field toward the Ag electrode, would be consumed by reacting with the diffused Ag particles. Such reaction not only triggers progressive ion dissociation and migration from the perovskite crystals, but also induces the corrosion of charge-transporting layer and Ag electrode. For the ITO-contact PVSCs, since the dissociated ions under light soaking would not be consumed, they would only accumulate at the perovskite/ITO interface and create an electrostatic force to oppose further ion dissociation and migration. Therefore, the amount of the I^- ions would be saturated, and the ions would be able to recover the V_i defects under the dark condition. In addition, it is expected that the vacancies close to the surface will be first recovered, and it hinders other ions from further diffuse into the bulk. Therefore, the ITO-contact PVSCs cannot be fully recovered even after resting under dark conditions.

To validate the above-proposed degradation mechanism in the Ag-contact and ITO-contact PVSCs, we investigated the stability of PVSCs under MPP tracking over light/dark cycling, and the corresponding device performance is shown in Figure 4a. Indeed, the ITO-contact PVSC exhibits harvesting–rest–recovery (HRR) cycles in which the device harvests solar energy under light condition, undergoes a rest phase under dark condition, and recovers its photovoltaic performance. On the contrary, the

Ag-contact PVSC does not show such HRR cycles as shown in Figure S6 (Supporting Information). The fast and unrecovered degradation observed in Ag-contact PVSCs is not only from the ion dissociation and migration in perovskite films, but also from the corrosion of Ag electrode due to the severe reaction between perovskite and Ag metal electrode. The HRR cycles observed only in the ITO-contact device provides strong evidence to support the above-proposed degradation mechanism. Most recently, with a robust Au electrode rather than Ag, Khenkin et al. also observed similar recovery performance of PVSCs when the degradation is less than 20%. The initial 20% device degradation can be ascribed to the metastable defect formation, and further degradation may involve in the reaction between Au and perovskite, which is irreversible.^[18] It should be noted that although there is a recovery process in ITO-contact PVSC, it cannot totally recover its initial performance. The PCE drops to about 90% of its initial value after 17 HRR cycles (350 h). Figure S7 (Supporting Information) shows the $J-V$ curves of each HRR cycle before and after the MPP tracking to investigate the change of device photovoltaic parameters. Interestingly, during each MPP tracking cycle, it is observed that the J_{sc} is reduced but the V_{oc} is increased. We find that such a change in the $J-V$ characteristics is due to the dissociation and migration of dissociated ions in perovskite layer under light soaking as evidenced in the following device capacitance measurement results.

Figure 4b shows the capacitance–voltage ($C-V$) results of the ITO-contact PVSC. It is clearly shown that, after light soaking

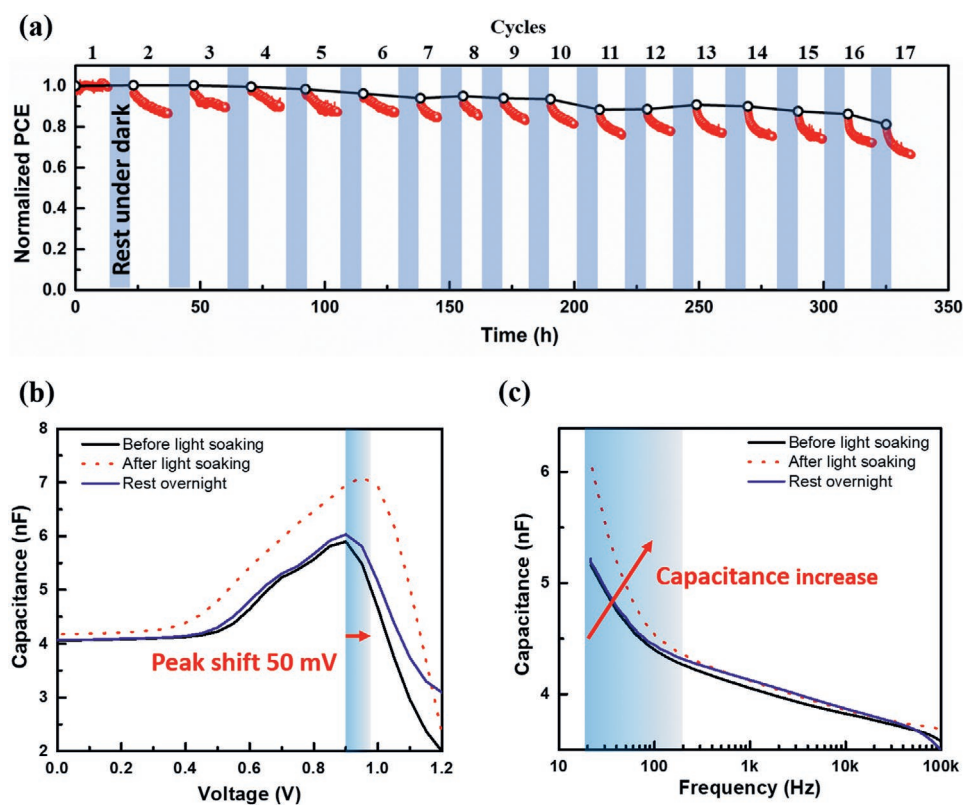


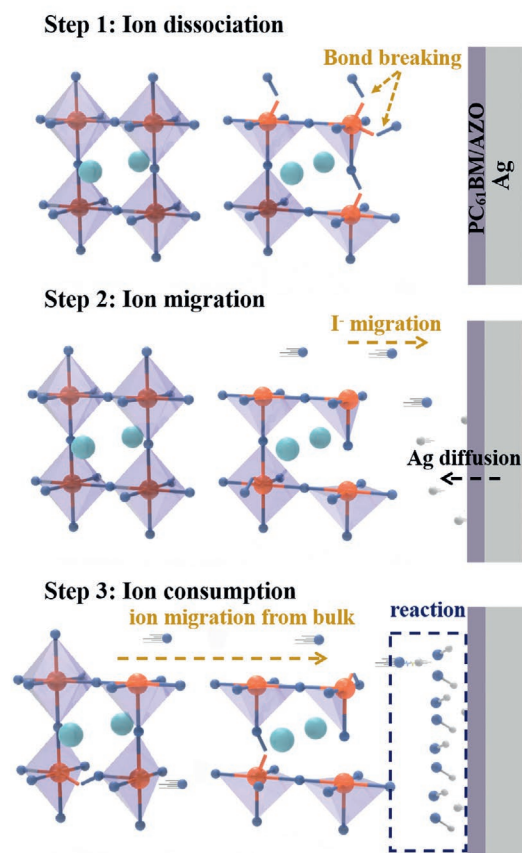
Figure 4. a) Normalized PCE of the ITO-contact PVSC under MPP tracking. The blue area is the resting phase during which the device is stored in dark condition. b) Capacitance–voltage and c) capacitance–frequency profiles of the ITO-contact PVSC before and after light soaking (10 h), as well as after resting in the dark overnight.

at MPP, the peak position of the device capacitance has been increased by 50 mV, indicating an increase of device built-in voltage (V_{bi}).^[19] Detailed discussion on the effect of ion dissociation on the change in V_{oc} and J_{sc} is provided in Figures S8 and S9 (Supporting Information). Moreover, as shown in Figure 4c, the capacitance–frequency (C – f) measurement result also supports the generation and recovery of ionic defects during MPP tracking. The device capacitance below 100 Hz increases after light soaking, where the capacitance at such low frequency is typically associated with the slow ionic response.^[20] Importantly, it should be noted that both C – V and C – f profiles of the ITO-contact PVSC recover to their initial states after resting in the dark overnight. Such capacitance recovery is also a direct piece of evidence for the self-healing of the dissociated ions to the corresponding vacancy states in perovskite lattices. As shown in Figure S10 (Supporting Information), the capacitance of the Ag-contact device in both C – V and C – f measurements significantly increases after light soaking and cannot be recovered after resting overnight. S-EQE, HRR cycle, and device capacitance measurement have excellent consistency with the proposed degradation mechanism of ion dissociation and recovery in PVSCs.

The above results provide strong fundamental understanding of the degradation mechanism caused by ion dissociation in PVSCs, as illustrated in Figure 5. First, light soaking initiates

the ion dissociation from perovskite lattices, and especially the mobile I^- ions are driven to the perovskite/electrode interfaces by the internal electrical field. Second, if the dissociated ions are consumed by reacting with the electrode as in the case in Ag-contact devices, this process would trigger a chain reaction to accelerate further ion dissociation from the perovskite bulk, inducing large amount of defects including vacancies, interstitials, and antisites. In contrast, if such a reaction could be prohibited as using ITO as the electrode, the dissociated ions would only accumulate at the device's interfaces without consumption, and the dissociated ions are able to restore the corresponding vacancies in the perovskite lattice under dark condition, enabling a long lifespan of device performance. It is worth mentioning that the degradation of perovskite is determined by combined effects from the electrode and perovskite materials. Different from other photovoltaic materials such as organic and silicon where the electrode-diffusion-induced degradation is not that severe, the ions in perovskite tend to be dissociated and trigger reaction with other materials. Therefore, stabilizing the ion coordination would be the ultimate strategy to achieve long-term stability. However, as shown in this study, PVSCs' performance could also be stabilized with an effective approach to prevent the dissociated ions from being consumed by reacting with other materials in device.

(a) Degradation of Ag-contact PVSCs



(b) Recovery of ITO-contact PVSCs to enhance stability

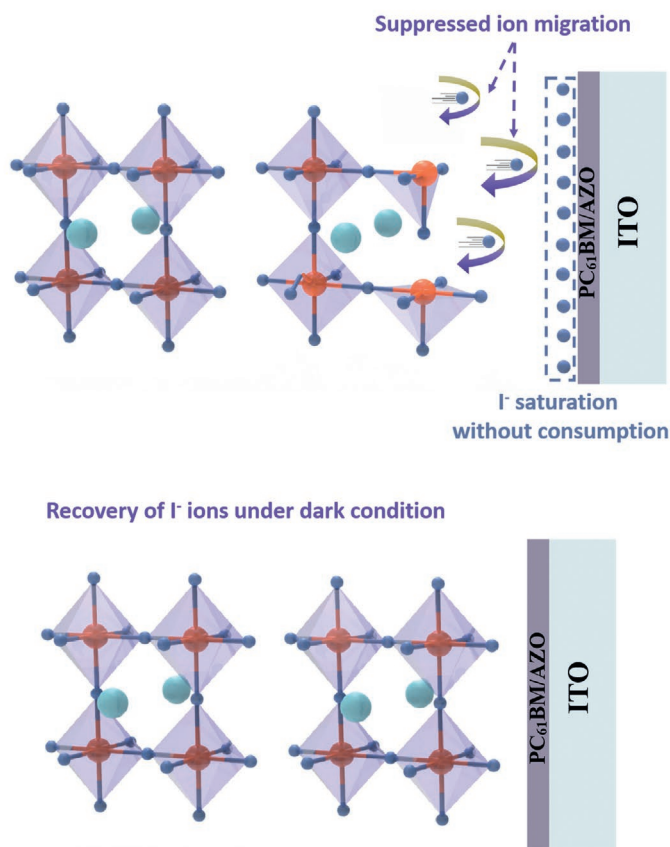


Figure 5. a) Schematic illustration of the degradation process in Ag-contact PVSCs including ion dissociation, ion migration, and ion consumption. b) Working principle of the ion dissociation and recovery process in ITO-contact PVSCs.

Experimental Section

Materials: NiO_x precursor material, nickel acetate tetrahydrate, (Ni(OAc)₂·4H₂O) was purchased from Sigma–Aldrich. Lead iodide (PbI₂) and methylammonium iodide (MAI) were bought from Tokyo Chemical Industry and GreatCell Solar, respectively. Electron-transporting material PC₆₁BM was bought from 1-Materials. BCP and AZO nanoparticles' inks were purchased from Sigma–Aldrich. All organic solvents used in this study were obtained from Sigma–Aldrich.

Fabrication of Perovskite Solar Cells: The Ag-contact PVSCs were fabricated based on the structure of glass/fluorine-doped tin oxide (FTO)/NiO_x/MAPbI₃/PC₆₁BM/BCP or AZO/Ag, while the ITO-contact PVSCs were fabricated based on the structure of glass/FTO/NiO_x/MAPbI₃/PC₆₁BM/AZO/sputtered ITO. To fabricate PVSCs, patterned commercial FTO glass substrates were first cleaned and then dried in oven at 70 °C. Before film deposition, the cleaned FTO glass was further treated by UV–ozone for 20 min. The fabrication of NiO_x and MAPbI₃ perovskite layers was introduced in the previous report.^[21] PC₆₁BM (25 mg mL⁻¹ in chlorobenzene) was spin-coated onto the top of MAPbI₃ layer at 4000 rpm for 40 s. For the BCP layer, its precursor solution (1 mg mL⁻¹ in ethanol) was spun with 4000 rpm for 40 s. For the AZO layer, its nanoparticle ink was spun at 4000 rpm for 40 s. For Ag-contact PVSCs, a 100 nm Ag electrode was deposited by thermal evaporation at a base pressure of 10⁻⁷ Torr. For ITO-contact PVSCs, 500 nm sputtered ITO was deposited at room temperature by DC magnetron sputtering at a working pressure of 2.0 × 10⁻³ mbar as reported in the previous work.^[22]

Characterizations: The scanning electron microscopy (SEM) image of the perovskite layer and EDX mapping were obtained on Philips XL30 FEG. The absorption profile of perovskite and transmittance profile of sputtered ITO were obtained from a commercial UV–vis–IR optical spectrophotometer (Agilent Technologies, CARY-7000). The current density–voltage (*J*–*V*) characteristics of PVSCs were measured with a Keithley 2400 series source meter under an AM 1.5G solar simulator (ABET TECHNOLOGIES, Sun 2000) with a power density of 100 mW cm⁻². For the shelf lifetime evaluation, the PVSCs were stored in a N₂-filled glovebox, and the *J*–*V* curves were obtained at set intervals. For the MPP tracking, the PVSCs were measured in a N₂-filled glovebox under constant light soaking at 100 mW cm⁻² (white light-emitting diode (LED) array), and the devices were maintained at their MPP during the measurement. For the HRR cycles, the devices were first measured at MPP under an AM 1.5G solar simulator (ABET TECHNOLOGIES, Sun 2000) with a power density of 100 mW cm⁻² for 10–14 h, and then rested overnight under dark in a N₂-filled glovebox for 10 h. The spectra of the solar simulator and white LED array for the measurements were recorded using a spectrometer (Ocean Optics (320–1120 nm)) as shown in Figure S11 (Supporting Information). The highly sensitive external quantum efficiency (s-EQE) spectra of PVSCs were obtained using a home-built setup. During the measurements, light from a 1000 W xenon arc lamp (Newport) passes through a monochromator (Zolix) and optical chopper (ThorLabs) before being focused on the device area. The generated photocurrent was amplified by a current amplifier (Standard Research SR570) and then collected by a lock-in amplifier (Standard Research SR830). The intensity of the light source was measured by calibrated silicon and germanium detectors (ThorLabs). To improve the sensitivity of the s-EQE, a collection of long-pass filters were employed to eliminate the contribution from second harmonic diffraction signals, and the measurements were done inside a black box to eliminate the ambient light. The s-EQE measurements were conducted immediately after light soaking for different times. The degradation test and s-EQE measurements were conducted on three batch devices and observed similar phenomena. The capacitance of PVSCs under different voltages and frequencies were measured with an impedance analyzer (HP4284A). The transient photocurrent of PVSCs was measured by applying a laser pulse (532 nm and 6 ns) on the devices, and the signal was captured by a digital oscilloscope.

Supporting Information

Supporting Information is available from the Wiley Online Library or from the author.

Acknowledgements

The Solar Energy Research Institute of Singapore (SERIS) was supported by the National University of Singapore (NUS), the National Research Foundation Singapore (NRF), and the Singapore Economic Development Board (EDB). S.-W.T. acknowledges the financial support from the Hong Kong Research Grants (CityU 11304420).

Conflict of Interest

The authors declare no conflict of interest.

Author Contributions

Y.C., X.L., and Z.G. contributed equally to this work. Y.C., S.-W.T., and F.L. conceived the idea and designed all the experimental work. Y.C., X.L., and M.L. fabricated the solar cells. Z.G., Z.Z., and H.-W.L. contributed to the s-EQE analysis. Y.C. wrote the manuscript and then S.-W.T., F.L., and A.G.A. revised the manuscript. The overall project was supervised by Y.C., S.-W.T., and F.L.

Keywords

degradation, indium tin oxide contact, ion consumption, ion dissociation, perovskite solar cells, self-healing, sub-bandgap external quantum efficiency

Received: September 9, 2020

Revised: November 18, 2020

Published online: December 9, 2020

- [1] a) R. F. Service, *Science* **2014**, *344*, 458; b) G. Hodes, D. Cahen, *Nat. Photonics* **2014**, *8*, 87; c) M. A. Green, A. Ho-Baillie, H. J. Snaith, *Nat. Photonics* **2014**, *8*, 506; d) X. Liu, Z. Yu, T. Wang, K. L. Chiu, F. Lin, H. Gong, L. Ding, Y. Cheng, *Adv. Energy Mater.* **2020**, *10*, 2001958.
- [2] N.-G. Park, *Adv. Energy Mater.* **2020**, *10*, 1903106.
- [3] a) Q. Dong, F. Liu, M. K. Wong, H. W. Tam, A. B. Djurišić, A. Ng, C. Surya, W. K. Chan, A. M. C. Ng, *ChemSusChem* **2016**, *9*, 2597; b) L. Shi, M. P. Bucknall, T. L. Young, M. Zhang, L. Hu, J. Bing, D. S. Lee, J. Kim, T. Wu, N. Takamura, D. R. McKenzie, S. Huang, M. A. Green, A. W. Y. Ho-Baillie, *Science* **2020**, *368*, eaba2412; c) Y. Cheng, Q.-D. Yang, L. Ding, *Sci. Bull.*, <https://doi.org/10.1016/j.scib.2020.08.029>.
- [4] J. You, L. Meng, T.-B. Song, T.-F. Guo, Y. Yang, W.-H. Chang, Z. Hong, H. Chen, H. Zhou, Q. Chen, Y. Liu, N. De Marco, Y. Yang, *Nat. Nanotechnol.* **2016**, *11*, 75.
- [5] N. Arora, M. I. Dar, A. Hinderhofer, N. Pellet, F. Schreiber, S. M. Zakeeruddin, M. Grätzel, *Science* **2017**, *358*, 768.
- [6] E. Bi, W. Tang, H. Chen, Y. Wang, J. Barbaud, T. Wu, W. Kong, P. Tu, H. Zhu, X. Zeng, J. He, S.-i. Kan, X. Yang, M. Grätzel, L. Han, *Joule* **2019**, *3*, 2748.
- [7] C. C. Boyd, R. Cheacharoen, K. A. Bush, R. Prasanna, T. Leijtens, M. D. McGehee, *ACS Energy Lett.* **2018**, *3*, 1772.
- [8] a) W. Ming, D. Yang, T. Li, L. Zhang, M.-H. Du, *Adv. Sci.* **2018**, *5*, 1700662; b) F. Behrouznejad, S. Shahbazi, N. Taghavinia, H.-P. Wu, E. W.-G. Diau, *J. Mater. Chem. A* **2016**, *4*, 13488.
- [9] H. Jin, E. Debroye, M. Keshavarz, I. G. Scheblykin, M. B. J. Roeflaers, J. Hofkens, J. A. Steele, *Mater. Horiz.* **2020**, *7*, 397.
- [10] a) W.-Q. Wu, P. N. Rudd, Z. Ni, C. H. Van Brackle, H. Wei, Q. Wang, B. R. Ecker, Y. Gao, J. Huang, *J. Am. Chem. Soc.* **2020**, *142*, 3989; b) Y. Ma, Y. Cheng, X. Xu, M. Li, C. Zhang, S. H. Cheung, Z. Zeng,

- D. Shen, Y.-M. Xie, K. L. Chiu, F. Lin, S. K. So, C.-S. Lee, S.-W. Tsang, *Adv. Funct. Mater.* **2020**, *30*, 2006802.
- [11] D. Meggiolaro, S. G. Motti, E. Mosconi, A. J. Barker, J. Ball, C. Andrea Riccardo Perini, F. Deschler, A. Petrozza, F. De Angelis, *Energy Environ. Sci.* **2018**, *11*, 702.
- [12] a) W. S. Yang, B.-W. Park, E. H. Jung, N. J. Jeon, Y. C. Kim, D. U. Lee, S. S. Shin, J. Seo, E. K. Kim, J. H. Noh, S. I. Seok, *Science* **2017**, 356, 1376; b) T.-H. Han, J.-W. Lee, C. Choi, S. Tan, C. Lee, Y. Zhao, Z. Dai, N. De Marco, S.-J. Lee, S.-H. Bae, Y. Yuan, H. M. Lee, Y. Huang, Y. Yang, *Nat. Commun.* **2019**, *10*, 520; c) J.-W. Lee, N.-G. Park, *Adv. Energy Mater.* **2020**, *10*, 1903249; d) X. Liu, Y. Cheng, B. Tang, Z. G. Yu, M. Li, F. Lin, S. Zhang, Y.-W. Zhang, J. Ouyang, H. Gong, *Nano Energy* **2020**, *71*, 104556.
- [13] a) H. Lee, C. Lee, *Adv. Energy Mater.* **2018**, *8*, 1702197; b) S. Svanström, T. J. Jacobsson, G. Boschloo, E. M. J. Johansson, H. Rensmo, U. B. Cappel, *ACS Appl. Mater. Interfaces* **2020**, *12*, 7212.
- [14] a) Y. Cheng, H.-W. Li, J. Qing, Q.-D. Yang, Z. Guan, C. Liu, S. H. Cheung, S. K. So, C.-S. Lee, S.-W. Tsang, *J. Mater. Chem. A* **2016**, *4*, 12748; b) Y. Cheng, M. Li, X. Liu, S. H. Cheung, H. T. Chandran, H.-W. Li, X. Xu, Y.-M. Xie, S. K. So, H.-L. Yip, S.-W. Tsang, *Nano Energy* **2019**, *61*, 496; c) Y. Shao, Z. Xiao, C. Bi, Y. Yuan, J. Huang, *Nat. Commun.* **2014**, *5*, 5784.
- [15] C. M. Sutter-Fella, D. W. Miller, Q. P. Ngo, E. T. Roe, F. M. Toma, I. D. Sharp, M. C. Lonergan, A. Javey, *ACS Energy Lett.* **2017**, *2*, 709.
- [16] a) G. Landi, H. C. Neitzert, C. Barone, C. Mauro, F. Lang, S. Albrecht, B. Rech, S. Pagano, *Adv. Sci.* **2017**, *4*, 1700183; b) D. W. Miller, G. E. Eperon, E. T. Roe, C. W. Warren, H. J. Snaith, M. C. Lonergan, *Appl. Phys. Lett.* **2016**, *109*, 153902; c) A. Kumar, A. Rana, N. Vashistha, K. K. Garg, R. K. Singh, *Sol. Energy* **2020**, *211*, 345.
- [17] A. Buin, P. Pietsch, J. Xu, O. Voznyy, A. H. Ip, R. Comin, E. H. Sargent, *Nano Lett.* **2014**, *14*, 6281.
- [18] M. V. Khenkin, A. K. M, I. Visoly-Fisher, S. Kolusheva, Y. Galagan, F. Di Giacomo, O. Vukovic, B. R. Patil, G. Sherafatipour, V. Turkovic, H.-G. Rubahn, M. Madsen, A. V. Mazanik, E. A. Katz, *ACS Appl. Energy Mater.* **2018**, *1*, 799.
- [19] a) Y. Cheng, H.-W. Li, J. Zhang, Q.-D. Yang, T. Liu, Z. Guan, J. Qing, C.-S. Lee, S.-W. Tsang, *J. Mater. Chem. A* **2016**, *4*, 561; b) P.-Y. Lin, T. Wu, M. Ahmadi, L. Liu, S. Haacke, T.-F. Guo, B. Hu, *Nano Energy* **2017**, *36*, 95.
- [20] a) B. Chen, M. Yang, X. Zheng, C. Wu, W. Li, Y. Yan, J. Bisquert, G. Garcia-Belmonte, K. Zhu, S. Priya, *J. Phys. Chem. Lett.* **2015**, *6*, 4693; b) P. Lopez-Varo, J. A. Jiménez-Tejada, M. García-Rosell, S. Ravishankar, G. Garcia-Belmonte, J. Bisquert, O. Almora, *Adv. Energy Mater.* **2018**, *8*, 1702772.
- [21] M. Li, X. Xu, Y. Xie, H.-W. Li, Y. Ma, Y. Cheng, S.-W. Tsang, *J. Mater. Chem. A* **2019**, *7*, 9578.
- [22] Y. Cheng, C. Xie, X. Liu, G. Zhu, H.-W. Li, S. Venkataraj, Z.-K. Tan, L. Ding, A. G. Aberle, F. Lin, *Sci. Bull.* **2020**, *65*, 607.